A whole system model framework to predict damage in turnouts

Citation for the original published paper (version of record):
Six, K., Sazgetdinov, K., Kumar, N. et al (2023). A whole system model framework to predict damage in turnouts. Vehicle System Dynamics, 61(3): 871-891.
http://dx.doi.org/10.1080/00423114.2021.1988116

VEHICLE SYSTEM DYNAMICS
https://doi.org/10.1080/00423114.2021.1988116

A whole system model framework to predict damage in turnouts

K. Six [a], K. Sazgetdinov [a], N. Kumar [a], G. Müller[a], D. Velic[b], W. Daves [b], R. Skrypnyk [c] and B.A. Pålsson [c]

[a]Virtual Vehicle Research GmbH, Graz, Austria; [b]Material Center Leoben Forschung GmbH, Leoben, Austria; [c]CHARMEC/Department of Mechanics and Maritime Sciences, Chalmers University of Technology, Gothenburg, Sweden

ABSTRACT

This paper presents a whole system model framework that enables a holistic prediction of accumulated track damage in railway turnouts. A modular approach allows for insight into the interaction of different damage mechanisms such as rail profile change due to the plastic deformation and wear as well as track settlement. The methodology focuses on the two most critical areas of the turnout in terms of damage: switch and crossing panels. It is shown that at the beginning of the service life of the turnout the running surface of the rails in these areas change significantly due to plastic deformation, which in turn increases the dynamic impact forces from passing vehicles. These impact forces cause vertical track settlement that is most pronounced in the crossing area. Track settlement introduces additional dynamics into the system leading to self-reinforcing behaviour. It is shown that the proposed methodology can predict accumulated track damage accounting for the coupling between different damage modes such as track settlement, rail profiles plastic deformation and wear. It can therefore be used for holistic assessment of turnouts e.g. in design optimisation studies.

ARTICLE HISTORY
Received 10 March 2021
Revised 21 September 2021
Accepted 23 September 2021

KEYWORDS
Turnout; switches and crossings; track damage; rail surface damage; track settlement; rail wear; plastic deformation; whole system modelling; multi-body dynamics (MBD); vehicle-track interaction (VTI)

Introduction

Railway turnouts (switches and crossings, S&C) are integral components of any rail network as they provide flexibility to the system by allowing trains to change between tracks. This functionality comes at a cost, however, as rail discontinuities in the switch and crossing panels cause dynamic load amplifications that lead to higher degradation rates and increased maintenance costs compared to the plain line.

Because of the complexity of the turnout itself, the complexity of the vehicle-track interaction in turnouts and the complexity of the degradation mechanisms present, the assessment and improvement of turnouts is challenging. Currently, this is mainly done in

CONTACT K. Sazgetdinov kamil.sazgetdinov@v2c2.at

an isolated manner meaning that researchers focus mostly on one damage mode at the time. For example, [1] focus on wear and plastic deformation at the crossing nose. In [2] research has been carried out focussing on track settlement in turnouts. Furthermore, noise and vibrations in turnouts have been frequently investigated [3,4]. However, interactions between different damage modes in turnouts have not been considered yet in the published literature. This is an important capability that allows for holistic optimisation of the turnout design. If the design is only optimised to mitigate one damage mode at a time, this could lead to sub-optimal solutions that provide improvements in one area but gives a worse performance in another.

One of the reasons why different interacting damage modes have not yet been considered is that it is computationally infeasible to have a single model that can handle everything. Thus, a smart combination of relevant submodules for each topic of interest is the only chance to advance.

Such a modular methodology – a whole system approach – is presented in this study with the focus on long-term track damage patterns in turnouts. The work starts with an overview of the proposed methodology and a detailed description of its submodules. This is followed by the presentation and discussion of the results generated using this approach. The work is completed with final conclusions.

Methodology for simulation of accumulated track damage

The methodology presented in this work is focusing on vertical track settlement and rail geometry changes due to wear and plastic deformation in the regions of the switch and crossing panels, see Figure 1. The methodology is based on the combination of submodules to predict the long-term evolution of these track damage patterns using an iterative approach (the track damage development over several MGT of traffic).

First, Multi-Body Dynamics (MBD) simulations with a full-vehicle model in combination with the initial track, initial rail profiles and 15 measured wheel profiles running over the turnout are carried out (the upper block in Figure 1). The variation of the wheel profiles represents different states of wheel wear running over the turnout. This is important because the impact forces occurring in the regions of the switch and crossing panels and therewith the evolution of the track damage are highly influenced by the shape of the wheel profiles [5,6]. These impact forces are also affected by the track stiffness distribution along the turnout which therefore needs to be considered in the MBD simulations. For the first MBD simulations (loop 1) a perfect track geometry is assumed, thus, dynamic wheel-rail contact forces are mainly affected by the combination of wheel and rail geometries. Two types of MBD simulations are carried out (see Figure 1). The low-speed MBD simulations are performed to get the vertical wheel trajectories (vertical kinematic movement of the wheel relative to a reference coordinate system) for all considered wheel profiles in the regions of the switch and crossing panels needed as an input for the following Vehicle-Track-Interaction model (VTI) calculations [7]. The VTI model is aimed at predicting the evolution of the vertical track geometry as a function of accumulated traffic load measured in MGT [7] (left bottom block in Figure 1). The dynamic MBD simulations are carried out to obtain the wheel-rail contact patch results (dimensions, normal and tangential creep forces, creepages, etc.) needed for the following rail wear and rail plasticity calculations to predict the rail profile evolution as a function of MGT (right bottom image in Figure 1).

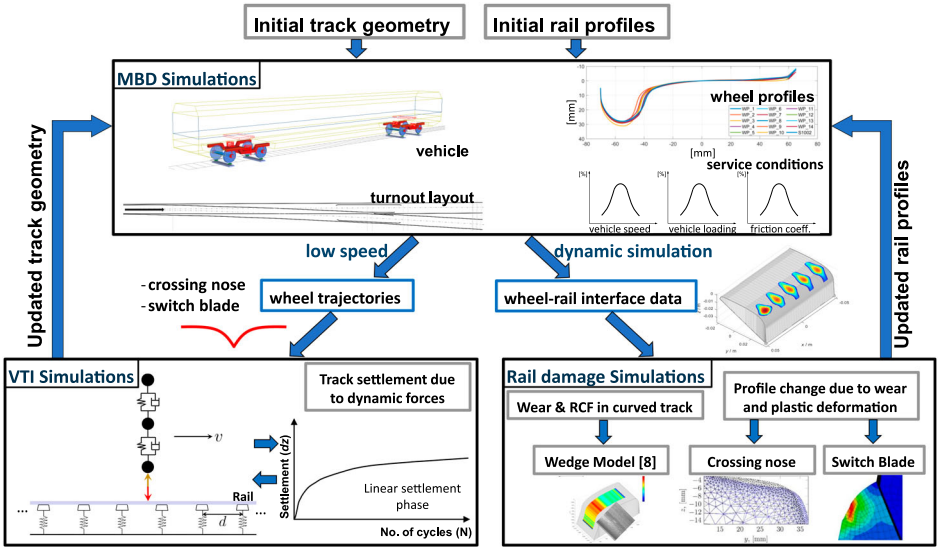

Figure 1. Whole system based methodology (WSM) for the track damage prediction in turnout. The initial track geometry and initial rail profiles are used as an input for the initialisation of the WSM operation. The subsequent cycles combine the results obtained from the different submodules - the updated track geometry from the VTI model and the updated rail profiles from the rail damage models - to predict the evolution of track damage with track service measured in MGT.

Other modules can be added, for example, a model to predict RCF crack initiation (wedge model [8–10]). However, such investigations are not presented in this work.

After finishing these calculations in the 1st loop, the predicted vertical track geometry from the VTI model (crossing and switch panel region) and predicted rail profiles (crossing nose and switch rail) are passed back to perform the MBD simulations in loop 2. This process of obtaining rail profile track geometry evolution and the exchange of the data between these two submodules is repeated until the defined traffic load is reached. In this demonstration of the methodology, two calculation loops are performed where are all damage states are updated, the first loop consists of simulations between 0–2 MGT and in the second loop 2–4 MGT of the traffic. Within each loop, much shorter iteration steps are used for each damage mode.

Results from these two loops are computed and compared for two different stiffness profiles along the turnout. One with constant stiffness and one with variable stiffness that accounts for the higher stiffness in the crossing panel region.

The next section gives a detailed description of the WSM submodules used for the prediction of the track damage evolution using the proposed methodology.

Modelling

For the track damage investigations performed in this work, 4 MGT of the traffic was simulated in two loops of 2 MGT each in the facing move meaning that the train is travelling from the switch towards the crossing. The traffic was simulated for the diverging (branching) route for the switch panel and for the through (straight) route in the crossing region.

Multi-body dynamics model

The main purpose of the MBD model within the WSM framework is to evaluate the static and dynamic vehicle-turnout interaction for the given turnout state and obtaining the wheel-rail contact data. The static and the dynamic interaction data are used as input for the VTI model and rail and track damage simulations blocks, respectively. The track model in the MBD model is created for the 60E1-760-1:15 turnout from the S&C simulation Benchmark [11] and the traffic on this track is represented from the passenger vehicle from the Manchester Benchmark [12]. The varying rail geometry is given by the sets of consecutive rail cross-sections along the length of the turnout. The track flexibility is represented via co-running track models – systems of masses, springs, and viscous dampers – that follow each wheelset.

As the purpose of this study is to demonstrate the evolution of accumulated damage as a function of traffic load, the base vehicle model has been simulated in combination with the set of different wheel profiles to better represent the variation in wheel profile geometry present in traffic. The set consists of 14 measured wheel profiles from Regina passenger trains in Sweden [5] and a nominal S1002 wheel profile. The full set of 15 wheel profiles is presented in Figure 2. The Regina profiles were chosen from a larger set of profiles with a spread in terms of their global conicity (normalised profile height difference between the running tread and field side) as this profile measure correlates strongly to the point of transition between wing rail and crossing nose [6]. Using the 15 wheel profiles and the simulation results of each of the 4 axle passages with the 11 tonnes axle load of the Manchester Benchmark vehicle, a set of simulations correspond to $15 \times 4 \times 11 = 660$ tonnes of traffic. This set of simulations is then repeated and extrapolated to reach a desired tonnage of traffic in damage calculations as described in coming subsections. The static and dynamic wheel-rail interaction data obtained from the MBD model are used as an input for the different damage models which are described next.

Wear and plasticity model for switch blade

The method presented within this section investigates the cyclic profile degradation of switch rails. A three-dimensional finite element (FE) model is utilised to calculate cyclic plastic deformation and wear caused by the contact loading between wheel and rail. This

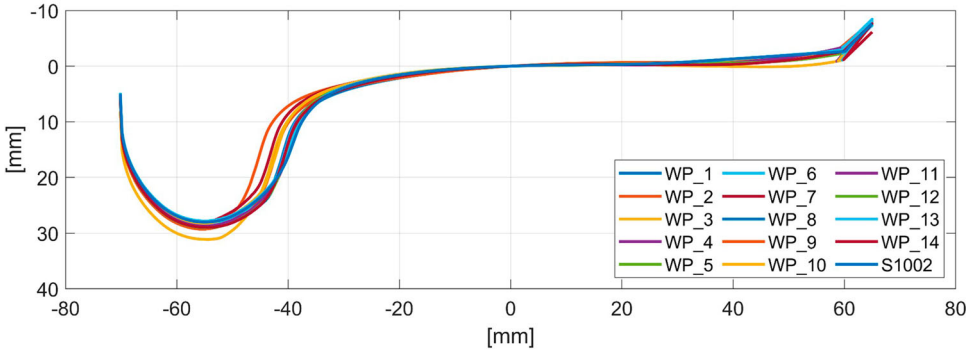

Figure 2. Sample of 14 measured and one nominal S1002 wheel profiles.

analysis evaluates the geometrical change of the switch rail, caused by wear and plastic deformation separately. The plastic deformation results in a shape change of the switch rail with volume constancy. The wear reduces the volume of the rail proportional to the contact loading. After a certain number of FE loading cycles, the nodal displacements due to wear and plastic deformation are superimposed. The hardness change due to varying plastification is not considered in the wear model. This is because needed measurement data are not available for the considered material yet (see also section *Wear and plasticity models for crossing nose*). However, such data can easily be considered in the methodology in the future. The approach enables the comparison of the geometry and volume change due to wear and the geometry change due to plasticity.

To reduce the calculation time to a minimum, the extrapolation methodology introduced in [13] is adapted and used in this analysis. The current analysis focuses on the curved switch rail of the diverging route. For the FE calculations the commercial software package ABAQUS 2019 is used and the postprocessing and extrapolation are conducted with Python 3 scripts.

The explicit FE model contains 1.5 m of the switch rail and the main stock rail from the diverging route. The track bedding is modelled by means of discrete spring-damper elements in the vertical and lateral direction with stiffness and damping parameters according to [14]. The static wheel load is applied as a nodal force on the wheel centre point and the masses and inertias of the wheelset, and the bogie are prescribed to reproduce a characteristic lateral loading on the switch rail. The vertical and lateral primary suspensions are implemented with vehicle parameters corresponding to the Manchester Benchmark vehicle model [12]. In order to produce a comparable loading situation, the same set of 15 wheel profiles introduced in subsection *Multi-Body Dynamics model* are utilised for the cyclic simulations.

Surface to surface contact is defined between the wheel and switch rail and between the wheel and stock rail. Additionally, contact is defined for the interface of the switch rail and the stock rail to allow for a relative motion between the two rails. The friction coefficient μ is set to 0.35 for all contact definitions, normal and tangential behaviour is solved utilising the hard contact and the penalty friction formulation, respectively. To account for cyclic plastic deformation of the switch rail the Chaboche material model [15] with combined isotropic and kinematic hardening is used for the switch rail. All other components are modelled as linear elastic. The material model parameters are calibrated with multiaxially loaded stress-controlled tests of a perlitic rail steel (R350HT) specimen. Figure 3 shows the structure and sequential order of the developed models and subroutines utilised for the calculation of cyclic rail degradation.

The FE model is used to calculate the representative amount of loading cycles Δn. After this, the nodal displacement vector D, the material response set $\varphi(t_i)$ which contains the stress tensor S, the equivalent plastic strain ϵ_{pl} for the isotropic and the back stresses tensors α_{kin} for the kinematic hardening are extracted for further processing. For the same number of cycles, the wear depth h according to Archard's wear law [16] is:

$$h = C_{press} \cdot s \cdot k/H \tag{1}$$

The necessary parameters for the wear depth calculation in Eq. 1, are the contact pressure C_{press}, the incremental sliding distance s, the hardness of the worn material H and a dimensionless wear coefficient k.

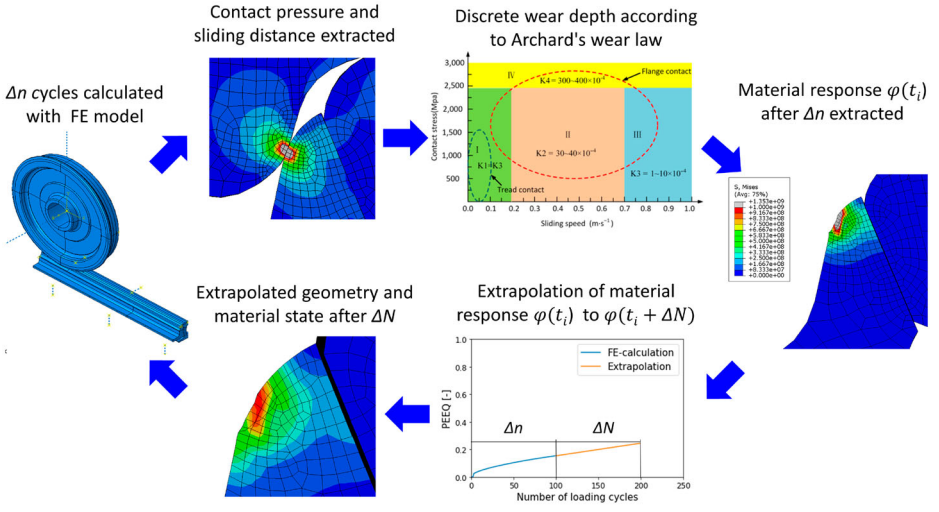

Figure 3. Schematic illustration of individual methods and models for extrapolation of switch rail profile degradation due to cyclic plastic deformation and wear.

The utilised extrapolation algorithm is based on a first-order Taylor series expansion ε_i, see Eq. 2. The algorithm evaluates the material response and the geometrical shape change caused by plastic deformation and wear during the numerically calculated loading cycles (Δn) and extrapolates these parameters for a predefined number of cycles (ΔN). After the extrapolation step, both material state and geometry are mapped on the cyclic FE model and further Δn cycles are calculated with the FE model. This procedure can be iteratively repeated until the maximum allowable geometry change, or a defined damage criterion of the rail is reached. The iterative approach is essential, to consider the changing contact conditions caused by the geometry change of the rail.

$$\varepsilon_{i+\Delta N} = \sum_{n=0}^{m} \frac{\Delta N^n}{n!} D_N^n \varphi(\tau_i) \tag{2}$$

The extrapolation starts with an initial extrapolation increment (ΔN_{start}) which is initially in the same range as the number of numerically calculated loading cycles (Δn_{start}) and is continuously increased after each extrapolation step until the $\Delta n/\Delta N$ ratio yields a ratio of 0.01. After the desired traffic MGT is reached for loop 1 (0-2 MGT), the updated switch rail profile cross-sections, together with the updated track geometry obtained from the VTI model (described in section *Evolution of vertical track geometry*) are passed back to perform the loop 2 (2-4 MGT) damage calculations for the switch, starting with the MBD simulation as shown in Figure 1.

Wear and plasticity models for crossing nose

Damage on the running surface of the crossing nose is simulated in terms of sliding wear and plastic deformation. Simulations of both damage mechanisms rely on the methodology described in [17].

Archard's model for sliding wear [16] is used together with Kalker's FASTSIM algorithm [18] to predict wear in the crossing nose. These methods are commonly used for the present application and are summarised in [1]. Due to repeated cyclic impact loading of the crossing nose, plastic deformation accumulates and can lead to substantial shape change. The amount of plastic deformation depends on the load and material response. Therefore, it is imperative to employ an accurate material model of material behaviour under cyclic plasticity. Here, the commonly applied Ohno-Wang model [19] formulated for small strains is used. Three back stresses (kinematic hardening variables) in the model are found to be sufficient (see [1]) to reach a reasonably good agreement with experimental data from uniaxial cyclic stress-controlled tests. A detailed description of the model and the material parameters can be found in [1]. Since the computational effort related to detailed 3D analysis to simulate long-term damage is very high, the simulations of plastic deformation are carried out for a number of selected 2D rail cross-sections. To further alleviate the computational expense, the load sequence produced by one passing of the vehicle is repeated multiple times to reach the desired amount of simulated traffic within one iteration of the methodology. Finally, the profile changes from the wear and plastic deformation are superimposed to produce the updated crossing rail profiles for the next iteration of the methodology.

In this study, a total of 4 MGT of traffic is simulated in two loops with an update of track geometry provided by the VTI model after 2 MGT as described previously. The prediction of rail profile degradation required an update of the MBD results every 0.01 MGT to avoid the formation of local geometry indentations that reinforce themselves. This means that the wheel-rail contact loads generated from the 15 vehicle passages with the wheel profiles of Figure 2 are repeated 15 times between rail profile updates.

The material parameters for the plasticity model are taken from [1] with the exception that the non-linear kinematic hardening was suppressed in the third back stress.

The Archard wear model depends on two material parameters: a non-dimensional wear coefficient that depends on sliding velocity and contact pressure and is often taken from a wear map [20] and hardness of the softer material. The wear coefficient has a highly non-linear dependence on the sliding velocity and the contact pressure where the wear coefficient typically increases with higher contact pressures [20] and higher sliding velocities [21]. For contacts on the crossing nose, the sliding velocity is typically low, but it reaches a maximum when the wheel is in simultaneous contact on the wing rail and crossing nose at different rolling radii during the transition between the rails. The contact pressure also varies significantly due to the transient impact loading on the crossing. Due to these varying contact conditions, it could be that the wear coefficient varies significantly during a wheel passage over a crossing, but a detailed wear map for the present material would be required to account for this effect. Unfortunately, wear data for the R350HT rail steel are scarce. Therefore, approximate and constant parameter values were chosen for demonstration purposes with a medium level wear coefficient of 3e-5 [20] and a hardness of 4.58 GPa. The latter corresponds to the nominal R350HT hardness of 3.5 GPa that has been scaled to resemble the run-in and hardened rails found in the track [22]. If a more detailed wear map was available, it would likely change the predicted wear distribution on the crossing nose with more wear in the locations with higher sliding velocities and higher pressures. Previous studies have shown, however, that a good qualitative agreement between measured and simulated profile change can be achieved also with a constant wear coefficient [17].

VTI model for track settlement

The VTI model [7] is used for the track settlement calculations in the region of the switch and crossing panels. A fast and reliable long-term track settlement prediction has been shown in [7] using the VTI model for large track sections (with the local track stiffness variation between 10 and 400 kN/mm). The model has two interacting components – vehicle and track, shown in the bottom left submodule block in Figure 1. The track model in the VTI model considers the discrete support of elastic rails on sleepers. In this way, the distribution of the dynamic loads from the wheel-rail interface to a certain number of sleepers can be described (dependent on the elasticity of the relevant components). Each sleeper can have its own stiffness and settlement behaviour. Dependent on the distribution of the stiffness and settlement behaviour along the track together with the initial track geometry, each sleeper settles dependent on the number of wheel passes (MGT). The dynamic loads depend on the vehicle properties. The vehicle model in the VTI model considers an eighth vehicle and is parameterised with the Manchester Benchmark dataset [12]. The track in the VTI model is initialised using the initial static track deflection and track geometry profiles along the turnout. Using a multivariable optimisation technique, the output of the initialisation step is the local stiffness and relative height for each sleeper along the track. On this initialised model, the vehicle moves with a constant speed and only vertical dynamics are considered.

The parameters for the track stiffness needed in the VTI model are established using the parameters list given in the S&C Benchmark [11] for modelling the switch and crossing region. The effective stiffness from this benchmark for the switch is found to be 72 kN/mm while for the crossing is 144 kN/mm. This doubled (higher) effective track stiffness for crossing is in accordance with the expected higher stiffness in this region [23–25] without the introduction of any elastic layers for stiffness adjustments. In this work, two different scenarios of stiffness profiles along the track are considered, as shown in Figure 4. In one case, a variable track stiffness profile has been chosen according to the design in the area of the crossing panel (between 72 and 144 kN/mm). In the second case, a constant track stiffness along the turnout has been assumed (72 kN/mm) representing a case where elastic under sleeper pads are used for optimising the track stiffness along the turnout, compensating the effect of varying length of sleepers and the crossing panel design [23,25].

The track geometry development predictions carried out in this work with the VTI model start with a perfect initial track geometry meaning that there are no track irregularities present when starting the calculations for loop 1. Using the considered track stiffness profile (Figure 4) and perfect initial track geometry, the VTI model is initialised, and the first wheel pass takes place. The dynamic interaction between wheel and rail is achieved via Hertzian springs with stiffness 5.13e-08 $N/m^{3/2}$ [26].

The evolution of track geometry depends on the settlement behaviour of the sleepers along the track due to the loads arising from the dynamic vehicle track interaction [27,28]. In this work, it is assumed that the track in operation is in the linear settlement phase of the tamping cycle and the sleeper settlement behaviour with wheel passes is represented by the Hettler model in its linearised form [27], described as:

$$dz_i = r_i F_{i,\,max}^{\alpha_i} \Delta N, \tag{3}$$

where $F_{i,max}$ is the maximum force in kN on the i^{th} sleeper during a wheel pass, ΔN is the number of wheel passes (linked to MGT), and r_i and α_i are local settlement parameters

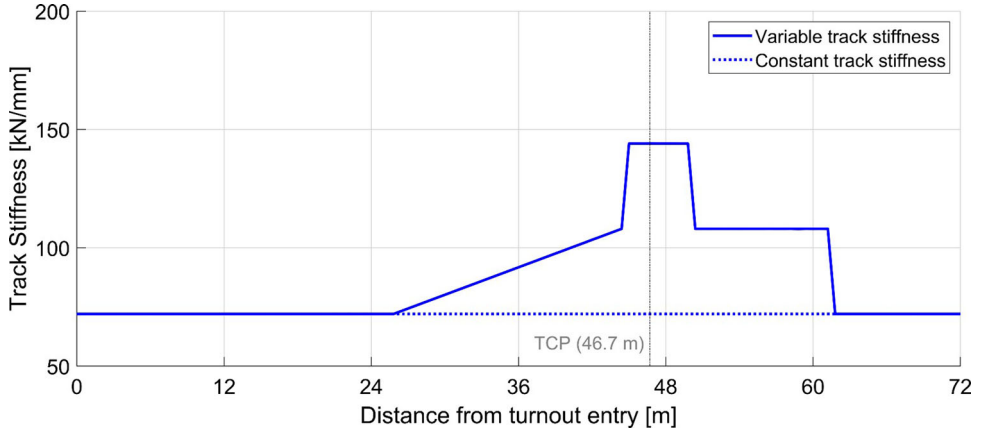

Figure 4. Assumed two different track stiffness profiles used for the VTI simulations according to the common Swedish turnout type [11]. In the case of constant track stiffness, a constant value of 72 kN/mm is assumed. For the variable track stiffness, a variation between 72 and 144 kN/mm is considered.

and are function of ballast and subsoil properties, operational history, etc. [7]. In this work, the parameters $\alpha_i = 1.6$ and $r_i = 1.93 \times 10^{-9} m/kN^{1.6}$ are taken directly from [7] for vertical track settlement calculations. The physical-based settlement model that is calibrated against the field measurements in [7] for a tangent track is applied in the turnout region.

All abovementioned WSM submodules (damage models for the switch and crossing panel) as well as the VTI track settlement model take the results from the MBD simulations as their input and pass the updated track geometry (from the VTI model) and rail geometries (from the rail damage wear and plastic deformation models for switch and crossing region) back to perform the next subsequent cycle of the MBD simulations in an iterative manner as shown in Figure 1. This is how the closed WSM loop is used to perform the accumulated track damage predictions. The results from the WSM loop are described in the next section.

Results

According to the methodology shown in Figure 1, two simulation loops are performed for calculating the track damage (wear, plastic deformation, and vertical track settlement). Each loop represents 2 MGT of traffic resulting in a total load of 4 MGT. Additional VTI simulations have been performed for higher MGTs without updating the rail profiles to get a better understanding of the influence of initial vertical track geometry on the track geometry evolution.

The following subsections below described the results of the whole system-based methodology in both switch and crossing nose area of the turnout.

Evolution of switch blade geometry

The methodology introduced in subsection *Wear and plasticity model for switch blade* was utilised to calculate 4 MGT of traffic in the diverging route. Figure 5 shows the lateral wheel force (Y – Force) on the switch rail for three different wheel profiles. It can be observed that

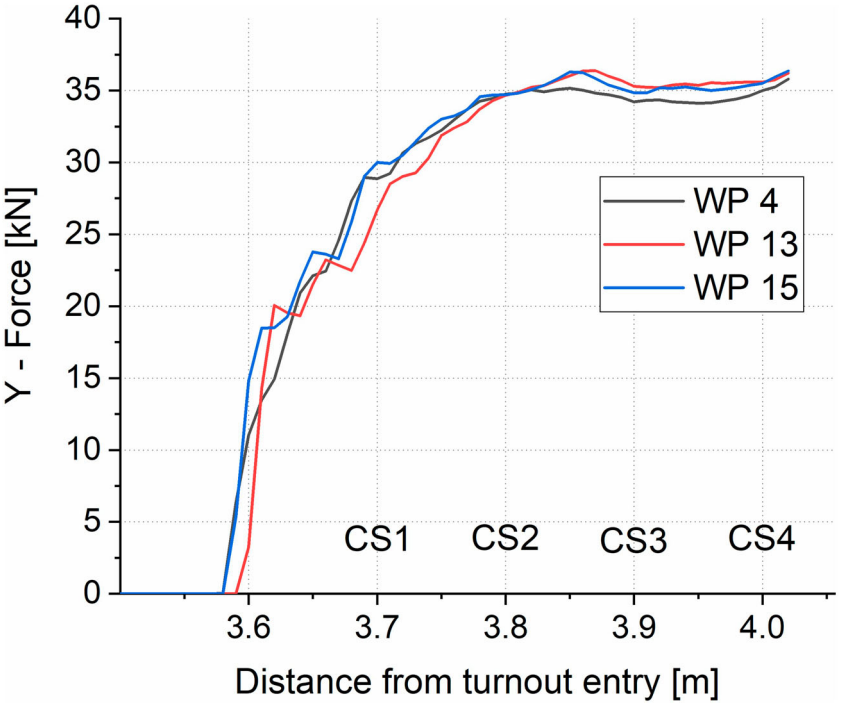

Figure 5. Lateral wheel force on switch rail for three various wheel profiles.

the force magnitude and the initial impact point on the switch rail are marginally affected for these wheel profiles.

The following results show the accumulated profile change for the switch rail at 3.7 - 4.0 m from the turnout beginning. In Figure 6 four specific cross-sections with 100 mm distance in between are compared after every MGT of traffic. A pronounced profile deterioration is prevalent within the initial MGT of traffic. After this run-in phase, the profile change is stabilised and progresses continuously with traffic. Furthermore, it can be observed that the profile deterioration increases with the longitudinal track position of the cross-section. This can be directly related to the lateral contact force curve and the position of the analysed cross-sections shown in Figure 5.

The profile deterioration of the switch rail is governed by plastic deformation and wear of the rail material. Figure 7 shows the accumulated shape change area caused by plastic deformation and the wear area according to Figures 8 and 9. It can be observed that the plastic deformation contributes a significant part to the total geometry change of the switch rail. To summarise, the shape change due to plastic deformation is the main mechanism for the rail damage in the switch region deformation in the early stage of the loading process (0-2 MGT).

Evolution of crossing nose geometry

This section presents results for the evolution in crossing nose geometry in the form of shape change area (geometry change due to plastic deformation) [17] and wear.

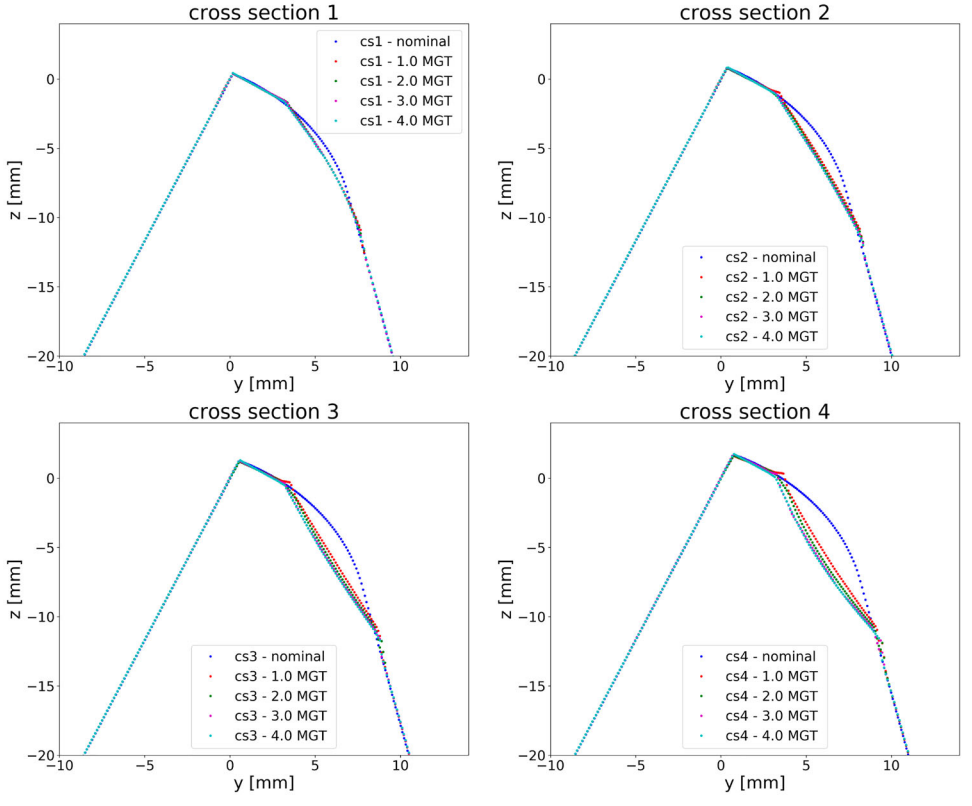

Figure 6. Nominal geometry and profile evolution of four cross-sections of switch rail in 100 mm distance for 4 MGT traffic load.

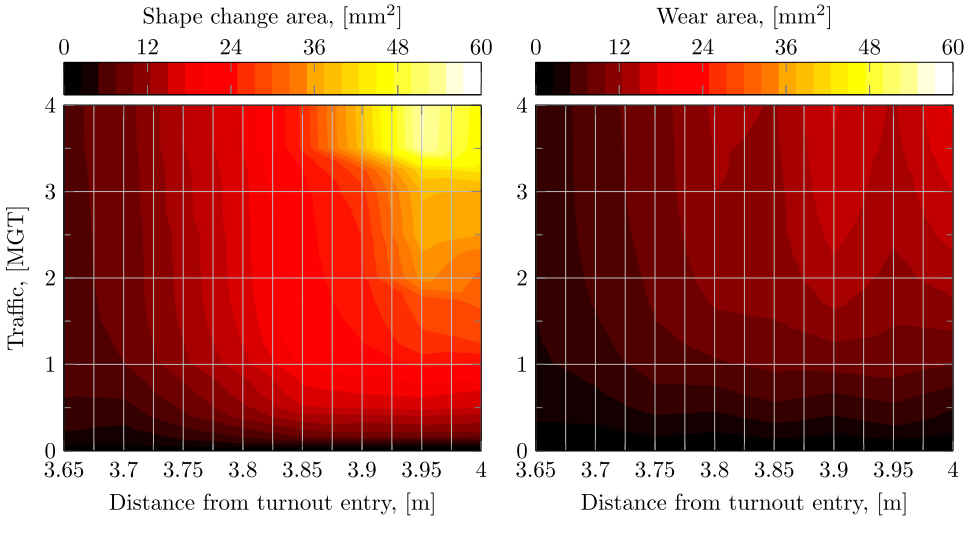

Figure 7. Accumulated shape change area due to plastic deformation and accumulated wear area over distance from turnout entry and traffic for the switch rail of the diverging route.

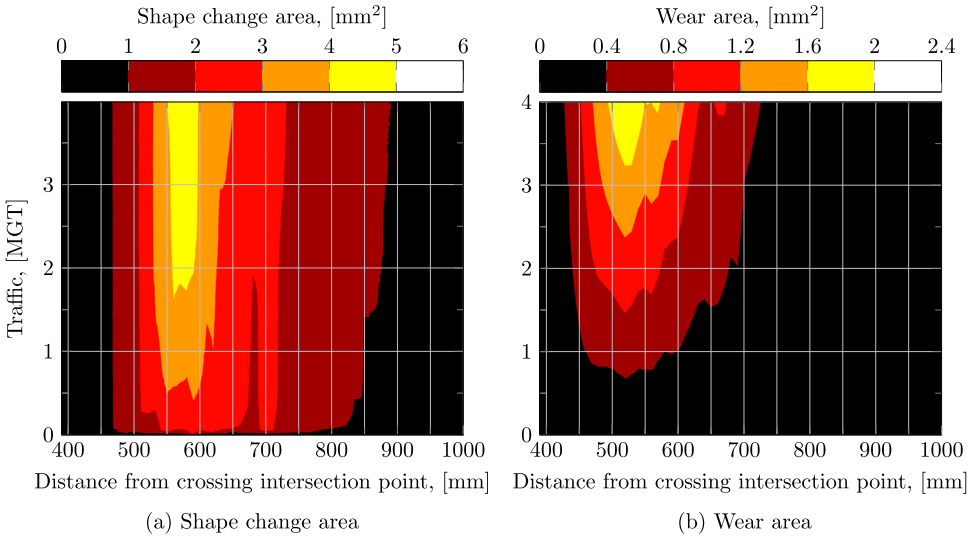

(a) Shape change area (b) Wear area

Figure 8. Shape change area and wear area distributions over the length of the crossing and simulated traffic in through route (variable track stiffness).

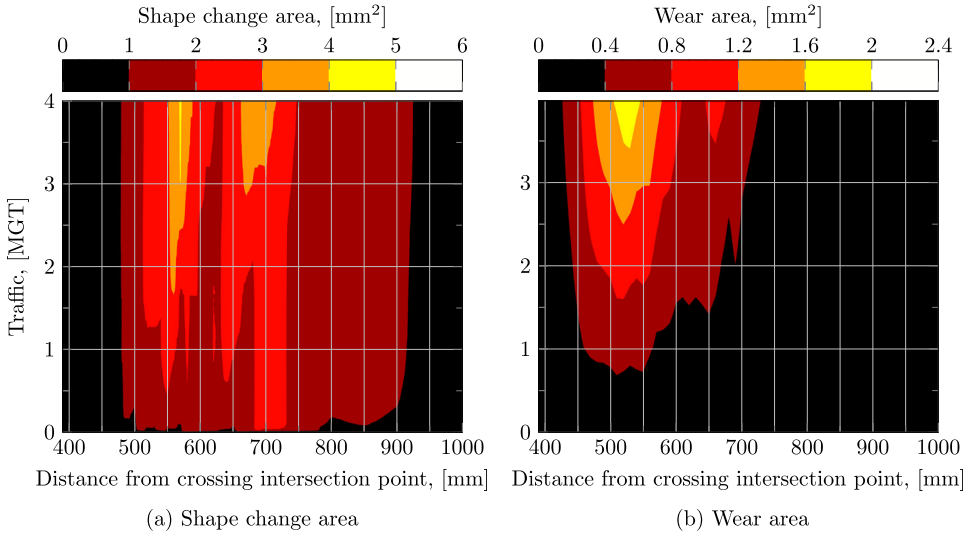

(a) Shape change area (b) Wear area

Figure 9. Shape change area and wear area distributions over the length of the crossing and simulated traffic in through route (constant track stiffness).

Figures 8 and 9 present the shape change area and wear development during the simulated 4 MGT of traffic for the cases of variable track stiffness and constant track stiffness, respectively (see Figure 4). Most of the deformation is concentrated in the region between 500 and 800 mm after the crossing intersection point (where the gauge corner lines of the through and diverging route cross). By comparing the results for the two track stiffness profiles, it can be noted that plastic deformation is the dominant damage mechanism in both cases for the simulated traffic load. For both track stiffnesses, a shape change area of up to

2 mm^2 is reached almost instantly to then settle for slower growth as the material hardens. The wear area on the other hand demonstrates a rather constant growth. Contrasting the results from the different stiffness profiles it can be observed that the variable stiffness profile with a higher track stiffness at the crossing results in a greater profile change due to higher wheel-rail contact loads and more plastic deformation. The wear is also slightly higher for the stiffer track, but the difference is less pronounced.

After simulating 2 MGT of traffic in loop 1, the track settlement predicted from the VTI model (updated track geometries) together with the updated rail profiles from both switch and crossing panels were included in the MBD model before simulating an additional 2 MGT in loop 2. The results shown in Figures 8 and 9 suggest that it had no significant effect on plastic deformation or wear. This is confirmed by the results calculated with the VTI model presented in subsection *Evolution of vertical track geometry*. A further result of this investigation is that wear has a smaller influence on rail profile evolution during the first 4 MGT of traffic compared to plastic deformation.

Evolution of vertical track geometry

This section presents the combined results regarding wear and plastic deformation as well as the track geometry degradation due to the dynamic wheel-rail contact force for both switch and crossing panels.

In this work, the through route is simulated for the crossing panel while the diverging route is simulated for the switch panel. The 15 vertical wheel trajectories for the set of measured wheel profiles at the beginning of loop 1 (0-2 MGT) are shown in Figure 10 (left column) obtained from the MBD simulations using the nominal rail profiles, as described in section *Multi-Body Dynamics model*. As expected, a distinct variation in the wheel trajectories can be seen for both regions. These wheel trajectories are then used as an input to perform the next subsequent cycle of the VTI simulations for analysing their effects on the dynamic wheel-rail contact forces and the track geometry evolution for both switch and the crossing regions. Figure 11 (left column) shows the corresponding wheel-rail contact forces for all considered wheel profiles in the switch and in the crossing panel (variable track stiffness case, see Figure 4) for loop 1. These results show that the shape of the wheel profiles strongly influences the wheel trajectories and therewith the dynamic wheel-rail contact forces for both switch and crossing panels. The dynamics in the contact forces are less pronounced for the switch compared to the crossing panel.

The right column in Figure 10 shows the wheel trajectories at the beginning of loop 2, obtained from the MBD simulations using the updated rail profiles from the wear and plastic deformation calculations for both switch and crossing panels discussed in the previous section. The results clearly show that the small changes in the rail profile shapes affect the wheel trajectories (see the right column in Figure 10) which in turn affects the dynamic wheel-rail contact forces (comparing the results from the left and right columns in Figures 10 and 11).

The methodology to calculate the evolution of track geometry using the VTI model is shown in Figure 12 for loop 1 (0-2 MGT) for two of the 15 considered wheel profiles (standard S1002 and measured WP3). The results belong to the crossing panel for the case of variable track stiffness (see Figure 4). WP3 was chosen among the other fifteen measured profiles as it showed the highest dynamics in contact forces among the other considered

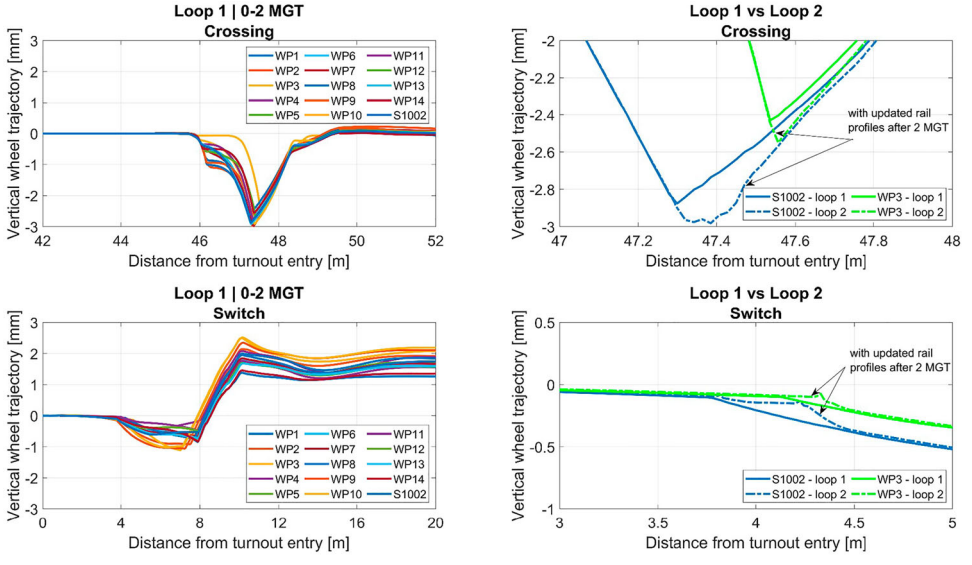

Figure 10. Wheel trajectories for the considered set of wheel profiles at the crossing and switch panels. Left: with initial rail profiles from loop 1, right: exemplary comparison of the wheel trajectories for initial rail profiles from loop 1 and updated rail profiles from loop 2 after 2 MGT of traffic.

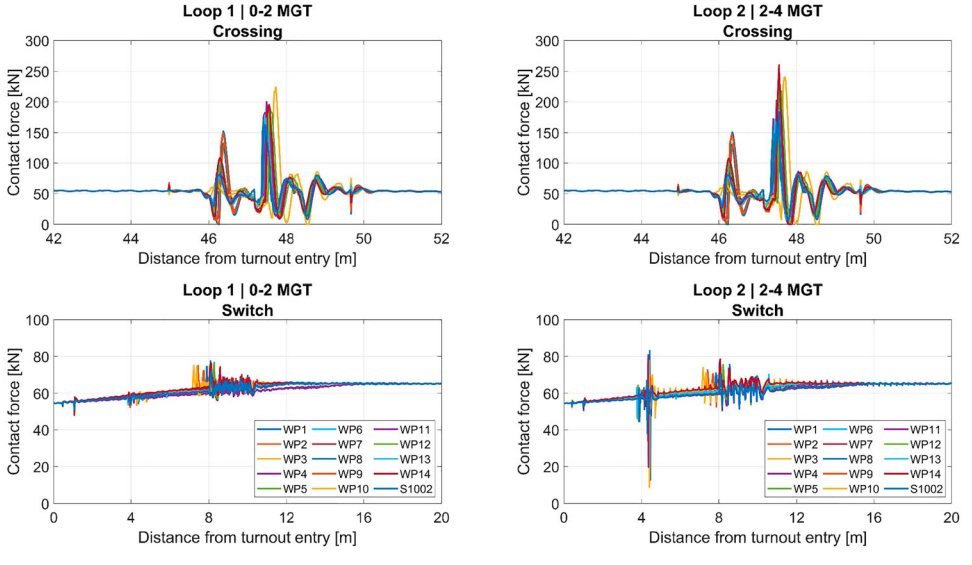

Figure 11. Wheel-rail contact forces for all considered wheel profiles at the crossing and switch panels. Left: with nominal rail profiles from loop 1, right: with updated rail profiles from loop 2 after 2 MGT traffic.

wheel profiles. After performing a wheel pass in the VTI simulation, the maximum force that the different sleepers experience is also extracted along the track, as shown in the third row in Figure 12. These maximum sleeper forces are then used in the settlement Eq. 3 to obtain the incremental sleeper settlement and thus, the evolution of the track geometry as shown in the fourth row in Figure 12. These vertical track geometry profiles are obtained

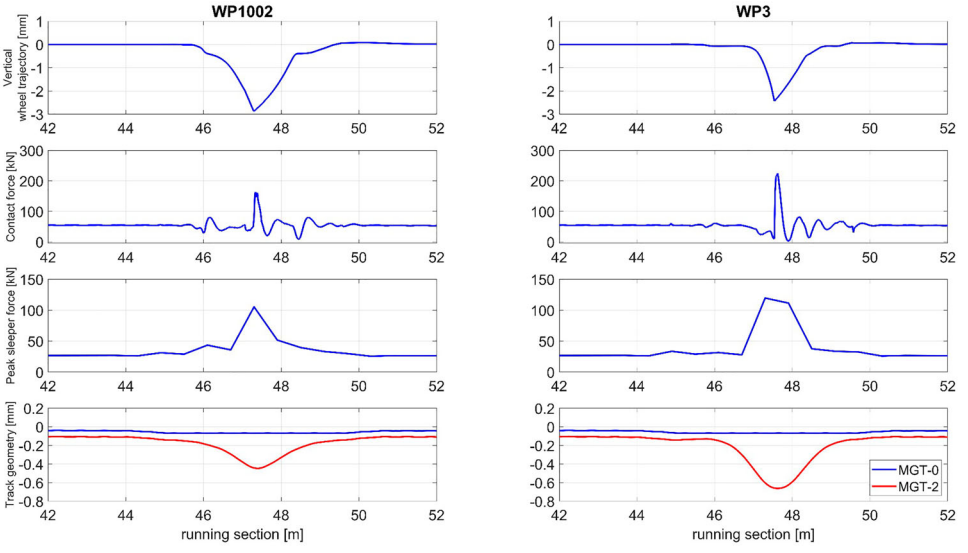

Figure 12. VTI model results for the crossing panel from loop 1 with nominal rail profiles. The first row represents the wheel trajectories for two chosen wheel profiles. The wheel-rail contact forces and the maximum sleeper forces after the first vehicle pass are shown in the second and third row, respectively. The evolution of vertical track geometry after 2 MGT of traffic from the corresponding wheel trajectories is shown in the fourth row.

under static loading conditions in a postprocessing step. The difference in the wheel-rail contact dynamics due to different wheel profiles affects the maximum sleeper force which in turn affects the evolution of the absolute vertical track geometry. The average of these different absolute track geometries is then used to calculate the relative track settlement after 2 MGT (and even further MGTs) of traffic for the wheel profiles mix used in this work. The relative track settlement after set traffic is simply calculated by subtracting the absolute track geometry value far to the left from the region of interest – where wheel profile variation does not contribute to any additional dynamics – from the absolute track geometry profile.

Figure 13 shows the relative track settlement results in the switch and crossing panel after 2 MGT of traffic for loop 1. Comparing to the switch panel, a higher settlement can be seen near the crossing panel due to higher dynamic contact forces (comparing top and bottom subfigures in Figure 11) and thus higher maximum sleeper forces in the crossing. The wavy characteristic visible for the switch case is due to the discrete sleeper location (higher vertical displacement when a vertical load is applied between sleepers). Note that such a characteristic is also present for the crossing case, but not visible due to the different y-axis range compared to the switch. Figure 13 also presents the results for the case of the constant track stiffness profile considered for the crossing (lower stiffness at the crossing area, see Figure 4). In this case, the relative track settlement develops slower compared to the variable track stiffness scenario due to reduced dynamic contact forces and lower maximum sleeper forces (load distribution to more sleepers).

After completing the loop 1 of the methodology (0-2 MGT), the output from the two submodules of the whole system model - rail profiles cross-sections (output from the rail

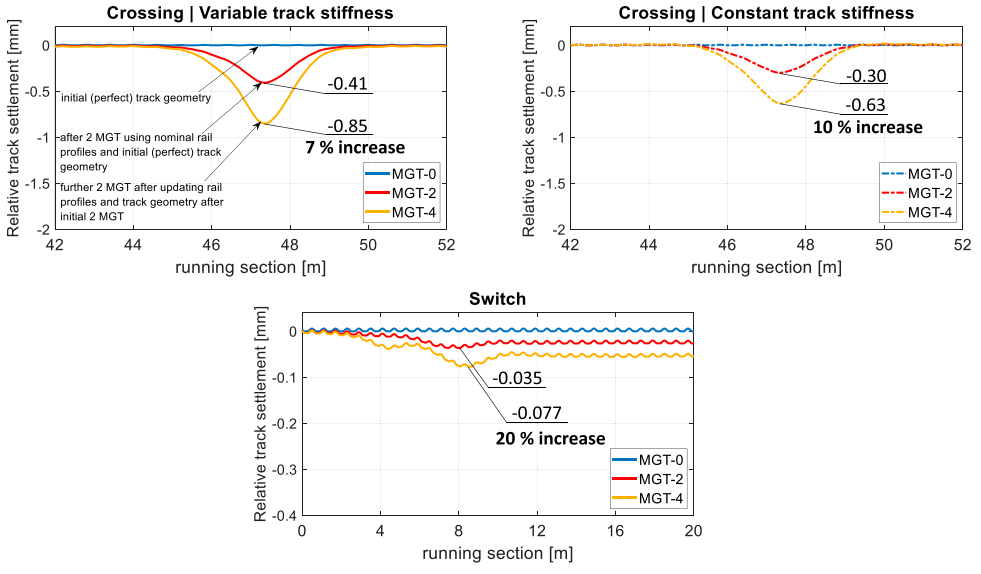

Figure 13. Evolution of relative track settlement from loop 1 and loop 2 after 2 and 4 MGT of traffic, respectively. Top row shows the results for the crossing panel with variable and constant track stiffness cases respectively, and the bottom figure shows the results for the switch panel. Note the different y-axis range for the switch panel.

damage simulations) and track geometries (output from the VTI settlement model) - are used as an input to start the next loop simulations (loop 2) to perform the further track damage prediction calculations, as shown in Figure 1 for the switch and the crossing regions. The track geometry development after loop 2 (4 MGT) describes the combined effects of both updated track geometry with the updated rail profile cross-sections as shown in Figure 13. In the same manner as in loop 1, a much lower relative track settlement is observed in the switch panel compared to the crossing panel for loop 2. For the switch panel, the track geometry after 4 MGT of traffic shows a wavier characteristic compared to the track geometry after 2 MGT. This is caused by changed dynamics due to the changed rail profile shapes resulting from loop 1. For the crossing panel, the results reveal that the change of track geometry is slightly higher in loop 2 (from 2 to 4 MGT) compared to loop 1 (from 0 to 2 MGT) (7% increase in the case of the variable track stiffness and 10% increase in the case of the constant track stiffness). The change in the wheel trajectories in loop 2 (shown in Figure 10) due to rail profile shape change leads to higher dynamic wheel-rail contact forces as shown in Figure 11. These increased dynamic forces are responsible for higher track settlement in loop 2 compared to loop 1. Higher track settlement in loop 2 compared to loop 1 is seen for both constant and variable track stiffness scenarios. An overall less settlement observed for the constant track stiffness compared to the variable track stiffness case is due to less dynamics in the wheel-rail contact force and better distribution of this force onto the sleepers.

Thus, the methodology presented here describes the interaction between different WSM submodules for predicting the long-term track damage patterns in turnouts and can assist in optimising this region in terms of reducing damage and maintenance activities.

Discussion

To better understand the interaction between the WSM submodules (rail profile shapes and vertical track geometry evolution) and their contribution on the further development of track damage pattern, additional VTI track settlement simulations up to 50 MGT were performed in the crossing area for the two design cases:

- Case 1 - VTI simulations using the nominal rail profiles only, and
- Case 2 - VTI simulations using the updated rail profiles after 2 MGT (initial setup of loop 2).

Case 1 assumes no rail profile shape change during the long-term track settlement predictions using the VTI model. On the other hand, Case 2 accounts for the rail profile change during the initial run-in phase till 2 MGT where most of the plastic deformation occurs. It is important to mention that not only track settles but also the rail profile shape changes during the service. However, in these investigations, it is assumed that the most change in the rail profile shape occurred till 2 MGT and is not significantly changing afterwards (see Figures 8 and 9). The idea is to present the effects of rail profile shape change on long term track settlement. These analyses are performed for both constant and variable track stiffness scenarios.

Figure 14 (left column) shows the evolution of the relative track settlement as a function of MGT for Case 1, starting with ideal initial track geometry and with nominal rail profiles, for both variable and constant track stiffness profiles scenarios. Figure 14 (right column) shows the evolution of the relative track settlement for Case 2, considering the updated rail profiles after the 2 MGT traffic. The results of the analysis (Figure 14) reveal that the variable track stiffness profile causes higher track degradation rates compared to the constant track stiffness. This is again due to less dynamics and better force distribution to the sleeper in the constant track stiffness scenario.

For both track stiffness profiles, the overall track settlement is higher for Case 2 than for Case 1, meaning that the contribution of the rail profiles change (updated rail profile) is higher on the long-term track geometry evolution. This because of the higher dynamics in wheel-rail contact force due to rail damage as seen in Figure 11 and is in accordance with the investigations performed in the previous section.

Figure 15 shows the minima of the relative track settlement profiles extracted from Figure 14. The results reveal a non-linear track settlement behaviour with MGT which is more pronounced for the variable track stiffness scenario. During the first 10–20 MGT of traffic, a quite linear behaviour can be observed meaning that the track geometry evolution is mainly driven by the wheel-rail impact forces caused by the wheel trajectories (rail profile in combination with wheel profile). This linear phase is followed by a non-linear region where the additional dynamics introduced by the track geometry start to play a role. This non-linearity can be interpreted as a self-reinforcing behaviour meaning that in the case of pronounced vertical track irregularities, they even further amplify their growth.

It is important to note that the focus of this work was on the development of a whole system based methodology for describing the interaction between the different track damage submodules. The absolute values of the predicted track settlement after 50 MGT of

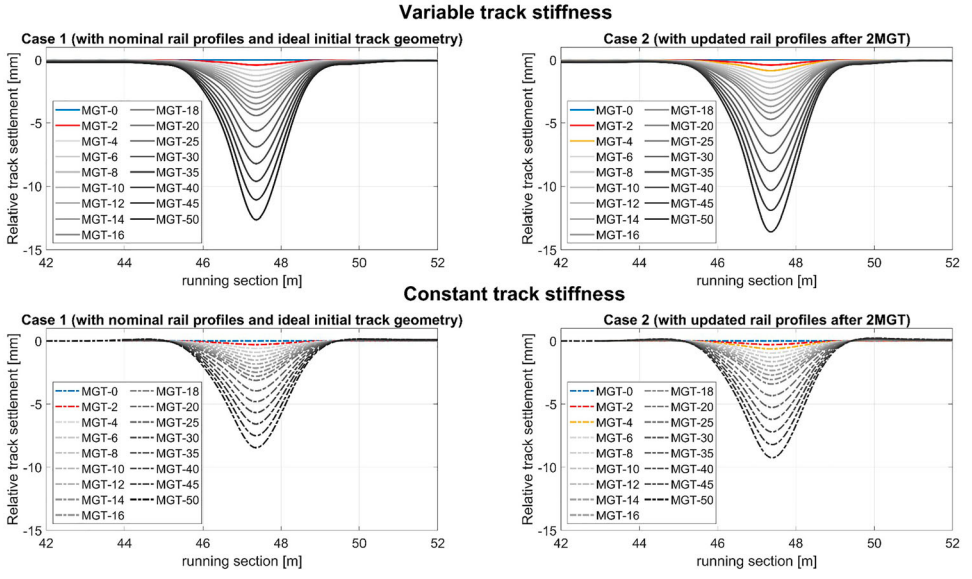

Figure 14. Evolution of the relative track settlement in the crossing panel. The top row shows the results for the variable track stiffness (Case 1 and Case 2 rail profile update) and continuing the VTI simulations up to 50 MGT of traffic. The bottom row shows the corresponding results for the constant track stiffness case.

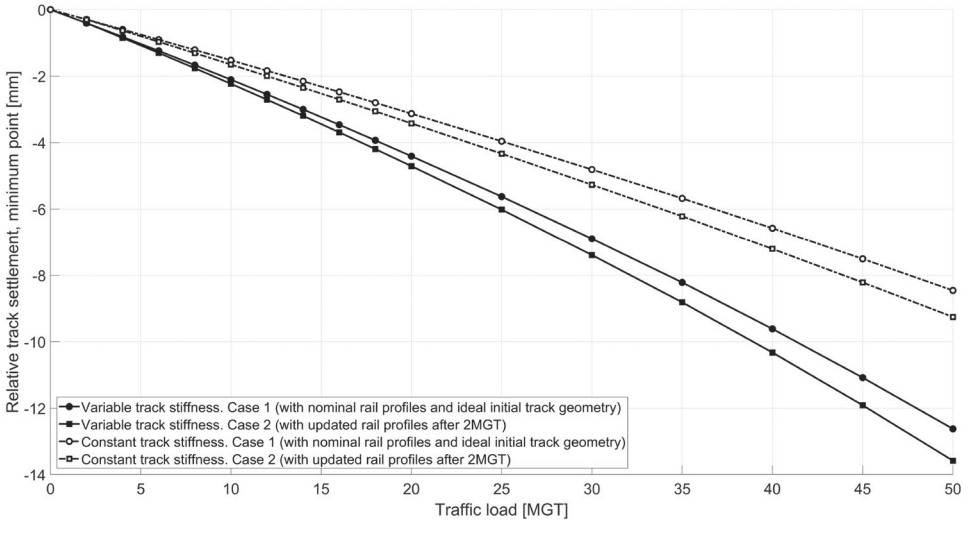

Figure 15. Evolution of the minimum point of the relative track settlement profiles taken from Figure 14 for up to 50 MGT traffic load in the crossing panel for the constant and variable track stiffness scenario.

traffic should only be seen as an indication even though the submodules used have been individually parameterised and validated. However, a validation of the presented overall methodology by means of field measurements is necessary and planned as the next further step.

Conclusions

In this work, a new whole system-based methodology has been presented to predict track damage in turnouts. The focus has been laid on rail profile change due to wear and plastic deformation for the R350HT rail material and vertical track settlement in the switch and crossing panels. In the region of the crossing panel two cases of track stiffness distribution along the track have been investigated: one case with a variable (increased) stiffness introduced by the varying length of the sleepers and the crossing panel; the second case with a constant stiffness for example realised by use of under sleeper pads. The following conclusions can be drawn:

- In loop 1 (0-2 MGT of traffic) a significant change of the rail profile shapes has been predicted in the switch and crossing area, mainly due to plastic deformation. After this run-in phase (until the material has hardened significantly), the rail profile geometry changes more slowly and wear becomes more predominant.
- The geometric rail discontinuities in the switch and crossing panels cause significant dynamic wheel-rail contact forces resulting in the development of vertical track irregularities. This effect is more pronounced in the crossing panel.
- Due to the plastic deformations occurring at the rail in the region of the crossing panel, the dynamic wheel-rail contact forces increase further resulting in a higher vertical settlement in loop 2 (2-4 MGT). The track irregularities resulting from the first loop (from 0 to 2 MGT) do not significantly contribute to the track settlement in loop 2 or to further plastic deformations and wear on the rails.
- For the switch panel, the settlement is higher in loop 2 due to plastic deformation and wear just like for the crossing. The dynamics wheel-rail contact forces are smaller than in the crossing panel, and therefore smaller vertical track settlement is observed.
- A lower track stiffness in the crossing panel (i.e. from the constant stiffness profile) region reduces plastic deformations and wear on the crossing and well as track settlement.
- With increasing amount of traffic and therewith increasing track irregularities and associated increasing wheel-rail contact forces respectively, the contribution of the actual track geometry to its future development increases, resulting in a self-reinforcing behaviour.
- The developed methodology accounts for the interaction of different damage phenomena and allows to improve turnout designs with regards to the considered track damage patterns (e.g. by designing track stiffness distribution along the track).

Although the modules of the whole system-based methodology are already well-validated, the overall methodology needs and planned to be further verified with field measurement data as the next step. Furthermore, it is planned to extend the methodology by further damage patterns, such as lateral track settlement and rolling contact fatigue driven cracks on rail surfaces.

Acknowledgement

The publication was partly written at Virtual Vehicle Research GmbH in Graz, Austria. The authors would like to acknowledge the financial support within the COMET K2 Competence Centres for

Excellent Technologies from the Austrian Federal Ministry for Climate Action (BMK), the Austrian Federal Ministry for Digital and Economic Affairs (BMDW), the Province of Styria (Dept. 12) and the Styrian Business Promotion Agency (SFG). The Austrian Research Promotion Agency (FFG) has been authorised for the programme management.

The publication was partly written at CHARMEC – Chalmers Railway Mechanics (www.chalmers.se/charmec) at Chalmers University of Technology in Göteborg, Sweden.

Disclosure statement

No potential conflict of interest was reported by the author(s).

Funding

This work was supported by Horizon 2020 Framework Programme: [grant number 826255].

ORCID

K. Six http://orcid.org/0000-0002-1005-8041
K. Sazgetdinov http://orcid.org/0000-0002-4126-493X
N. Kumar http://orcid.org/0000-0003-4867-1543
W. Daves http://orcid.org/0000-0002-2397-9704
R. Skrypnyk http://orcid.org/0000-0001-7180-7280
B.A. Pålsson http://orcid.org/0000-0002-2237-8560

References

[1] Skrypnyk R, Ekh M, Nielsen JCO, et al. Prediction of plastic deformation and wear in railway crossings - comparing the performance of two rail steel grades. Wear. 2019 Jun 15;428:302–314.
[2] Li X, Nielsen JCO, Palsson BA. Simulation of track settlement in railway turnouts. Veh Syst Dyn. 2014;52:421–439.
[3] Thompson DJ. Railway noise and vibration: mechanisms, modelling and means of control. 1st ed. Amsterdam Boston: Elsevier; 2009.
[4] Nielsen JCO, Lombaert G, Francois S. A hybrid model for prediction of ground-borne vibration due to discrete wheel/rail irregularities. J Sound Vib. 2015 Jun 9;345:103–120.
[5] Palsson BA, Nielsen JCO. Track gauge optimisation of railway switches using a genetic algorithm. Veh Syst Dyn. 2012;50(S1):365–387.
[6] Pålsson BA. A linear wheel–crossing interaction model. Proceedings of the Institution of Mechanical engineers. Part F: Journal of Rail and Rapid Transit. 2018;232(10):2431–2443.
[7] Kumar N, Six K. An efficient physical-based method for predicting the long-term evolution of vertical railway track geometries. Proceedings of the Institution of Mechanical engineers, part F: Journal of Rail and Rapid transit. 2021 (Accepted article. To appear at doi:10.1177/09544097211024803).
[8] Trummer G, Six K, Marte C, et al. An approximate model to predict near-surface ratcheting of rails under high traction coefficients. Wear. 2014 Jun 15;314(1-2):28–35.
[9] Trummer G, Marte C, Dietmaier P, et al. Modeling surface rolling contact fatigue crack initiation taking severe plastic shear deformation into account. Wear. 2016 Apr 15;352-353:136–145.
[10] Six K, Mihalj T, Marte C, et al. Rolling contact fatigue behaviour of rails: wedge model predictions in T-gamma world. P I Mech Eng F-J Rai. 2020 Nov;234(10):1335–1345.
[11] Bezin Y, Pålsson BA. Multibody simulation benchmark for dynamic vehicle-track interaction in switches and crossings: modelling description and simulation tasks. Veh Syst Dyn. 2021; doi:10.1080/00423114.2021.1942079.

[12] Iwnicki S. Manchester benchmarks for rail vehicle simulation. Veh Syst Dyn. 1998 Sep;30(3-4):295–313.
[13] Johansson G, Ekh M. On the modeling of large ratcheting strains with large time increments. Eng Comput. 2007;24(3-4):221–236.
[14] Nielsen JCO, Palsson BA, Torstensson PT. Switch panel design based on simulation of accumulated rail damage in a railway turnout. Wear. 2016 Nov 15;366:241–248.
[15] Chaboche JL. On some modifications of kinematic hardening to improve the description of Ratchetting effects. Int J Plast. 1991;7(7):661–678.
[16] Archard JF. Contact and rubbing of flat surfaces. J Appl Phys. 1953;24(8):981–988.
[17] Skrypnyk R, Ossberger U, Pålsson BA, et al. Nielsen Long-term rail profile damage in a railway crossing: field measurements and numerical simulations. Wear. 2021;472; doi:10.1016/j.wear.2020.203331.
[18] Kalker JJ. A fast algorithm for the simplified theory of rolling-contact. Veh Syst Dyn. 1982;11(1):1–13.
[19] Ohno N, Wang JD. Kinematic hardening rules with critical state of dynamic recovery.1. formulation and basic features for Ratchetting behavior. Int J Plast. 1993;9(3):375–390.
[20] Jendel T. Prediction of wheel profile wear-comparisons with field measurements. Wear. 2002 Jul;253(1-2):89–99.
[21] Lewis R, Olofsson U. eds. Wheel-rail interface handbook. Boca Raton, FL and Oxford: CRC Press and Woodhead Publishing; 2009.
[22] Schilke M, Larijani N, Persson C. Interaction between cracks and microstructure in three dimensions for rolling contact fatigue in railway rails. Fatigue Fract Eng M. 2014 Mar;37(3):280–289.
[23] Xu JM, Wang P, Ma XC, et al. Stiffness characteristics of high-speed railway turnout and the effect on the dynamic train-turnout interaction. Shock Vib. 2016;(1):1–14.
[24] Grossoni I, Bezin Y, Neves S. Optimisation of support stiffness at railway crossings. Veh Syst Dyn. 2018;56(7):1072–1096.
[25] Palsson BA, Nielsen JCO. Dynamic vehicle-track interaction in switches and crossings and the influence of rail pad stiffness - field measurements and validation of a simulation model. Veh Syst Dyn. 2015 Jun 3;53(6):734–755.
[26] Lei X. High speed railway track dynamics. Singapore: Springer; 2017.
[27] Hettler A. Bleibende Setzungen des Schotteroberbaus. Eisenbahntechnische Rundschau. 1984;33(11):847–854.
[28] Kumar N, Suhr B, Marschnig S, et al. Micro-mechanical investigation of railway ballast behavior under cyclic loading in a box test using DEM: effects of elastic layers and ballast types. Granul Matter. 2019 Nov;21(106):1–17.